Technical University of Denmark

DTU

Symmetry, vibrational energy redistribution and vibronic coupling: The internal conversion processes of cycloketones

Kuhlman, Thomas Scheby; Sauer, Stephan P.A.; Sølling, Theis I.; Møller, Klaus Braagaard

Link back to DTU Orbit

DTU Library
Technical Information Center of Denmark

Symmetry, vibrational energy redistribution and vibronic coupling: The internal conversion processes of cycloketones

Thomas S. Kuhlman, Stephan P. A. Sauer, Theis I. Sølling, and Klaus B. Møller

Symmetry, vibrational energy redistribution and vibronic coupling: The internal conversion processes of cycloketones

Thomas S. Kuhlman,[1] Stephan P. A. Sauer,[2] Theis I. Sølling,[2] and Klaus B. Møller[1,a)]

[1]*Department of Chemistry, Technical University of Denmark, Kemitorvet 207, DK-2800 Kgs. Lyngby, Denmark*
[2]*Department of Chemistry, University of Copenhagen, Universitetsparken 5, DK-2100 København Ø, Denmark*

In this paper, we discern two basic mechanisms of internal conversion processes; one direct, where immediate activation of coupling modes leads to fast population transfer and one indirect, where internal vibrational energy redistribution leads to equidistribution of energy, i.e., ergodicity, and slower population transfer follows. Using model vibronic coupling Hamiltonians parameterized on the basis of coupled-cluster calculations, we investigate the nature of the Rydberg to valence excited-state internal conversion in two cycloketones, cyclobutanone and cyclopentanone. The two basic mechanisms can amply explain the significantly different time scales for this process in the two molecules, a difference which has also been reported in recent experimental findings [T. S. Kuhlman, T. I. Sølling, and K. B. Møller, ChemPhysChem. **13**, 820 (2012)]. © *2012 American Institute of Physics*. [http://dx.doi.org/10.1063/1.4742313]

I. INTRODUCTION

With the use of ultrashort laser pulses, excited-state processes in molecules can be initiated with energy deposited in very specific regions of phase space and the resulting excited-state reaction dynamics can exhibit significant non-ergodic nature.[1,2] This non-ergodicity can be even more pronounced when the Born-Oppenheimer approximation breaks down and ultrafast population transfer between adiabatic states occurs mediated by crossings of two adiabatic potential energy surfaces,[3,4] i.e., the ubiquitous conical intersections.[5–7] Such processes are inherently different from their ground state counterparts. For ground state processes, internal vibrational energy redistribution (IVR) is often effective on a time-scale shorter than the rate of reaction as assumed by Rice-Ramsperger-Kassel-Marcus (RRKM) theory.[8] For excited-state processes, however, energy might not be redistributed between reactive and non-reactive bath degrees of freedom (DOF), and detailed analysis of the dynamics is required for determining the time-scale of reaction.[2]

If the coupling between two states is not strong enough to entail the presence of conical intersections but surface touchings or avoided crossings are present[9]—such as for the cases treated in this paper—perturbative approaches can be employed. Fermi's golden rule,[10]

$$w_{l \leftarrow m}(E) = \frac{2\pi}{\hbar} |\langle \psi_l | W | \psi_m \rangle|^2 \, \rho_l(E), \qquad (1)$$

gives the rate of transition between the initial state $|\psi_m\rangle$ and the final state $|\psi_l\rangle$ as induced by the perturbation W. $\rho_l(E)$ is the vibrational density of states (DOS) of the final state. From Eq. (1), one would intuitively expect that a change in the vibrational DOS would lead to a corresponding change in the rate of transition, however, this neglects the influence of a possible dependence of W on specific nuclear DOF. Furthermore, it is not discernible beforehand whether IVR is effective on the time-scale of the transition and, thus, whether or not ergodicity prevails. Whence, although Eq. (1) seems to provide qualitative predictions on the relative rate of, e.g., internal conversion processes in related molecules, to understand the true nature of such processes, a more detailed picture is necessary—a picture, which can only be inferred from dynamics simulations. In this work, we use two cycloketones, cyclobutanone and cyclopentanone, as model systems to investigate excited-state internal conversion and obtain such a picture.

The excited-state dynamics of cycloketones following excitation to a Rydberg state has been extensively investigated using different femtosecond time-resolved techniques and theoretical methods.[1,11–17] Initial processes involve internal conversion from a Rydberg state to the $(n, \pi*)$ state, the lowest lying excited singlet state. This is sometimes referred to as predissociation dynamics due to the eventual fate of the molecules. In the case of cyclobutanone and cyclopentanone, the internal conversion process has been investigated following excitation specifically to the $(n, 3s)$ Rydberg state using time-resolved mass spectrometry (TR-MS) (Refs. 14 and 17) and time-resolved photoelectron spectroscopy (TR-PES).[17] The latter study observed a marked difference for the two molecules in the time-scale for the internal conversion with the ratio of the two being 2:13 for cyclobutanone relative to cyclopentanone.[17]

To investigate the nature of this internal conversion process for cyclobutanone and cyclopentanone following excitation to the $(n, 3s)$ state, we present herein the construction of a high-order, five-dimensional model Hamiltonian for the two molecules and its subsequent use in a wave packet study of the internal conversion dynamics. Using this model Hamiltonian, we are able to investigate the precise nature of the vibrational motion inducing the transition between the initially prepared Rydberg state and the lower lying $(n, \pi*)$ state, i.e.,

a)Electronic mail: klaus.moller@kemi.dtu.dk.

the vibronic coupling represented in Eq. (1) as the perturbation operator W coupling the initial state $|\psi_m\rangle$ with the final state $|\psi_l\rangle$. The calculations are carried out in the diabatic representation, thus, W is an operator of coordinate dependent potential couplings, see Eq. (5), and not derivative couplings as in the adiabatic representation. This investigation inherently touches upon the role of internal vibrational energy redistribution (IVR) in the process of the internal conversion. The timescales obtained from the wave packet simulations show the same trend of timescales as observed experimentally. However, one would need to include time-resolved fields as well as the final cationic state (onto which the wave packet is projected in the pump-probe experiments) to fully simulate the experimental observable in order to obtain a more quantitative agreement between theory and experiment. Nonetheless, the present study reveals a clear picture that provides a deeper understanding of the experimental findings.

II. THEORY AND COMPUTATIONAL METHODS

A. Quantum dynamics

The fully quantum nuclear dynamics calculations performed in this work use the Multi-configuration time-dependent Hartree approach (MCTDH). In MCTDH, the wave function is written as a multi-configurational sum over Hartree products of single particle functions.[18–20] In the applications of this paper, we include four electronic states and the total wave function is given by

$$|\Psi(t)\rangle = \sum_{m=1}^{4} |\psi_m(t)\rangle, \qquad (2)$$

where each state $|\psi_m(t)\rangle$ is expanded in the MCTDH form. The summation index m refers to the ground state ($m = 1$), and the three excited states; the (n, π^*) state and the $(n, 3s)$ and lowest $(n, 3p)$ Rydberg state ($m = 2, 3, 4$).

MCTDH calculations were performed using the Heidelberg MCTDH code[21] version 8.4 Revision 6 in the multi-set formalism. The nuclear DOF correspond to dimensionless normal mode coordinates and were chosen as a subset of the full $3N - 6$ internal DOF of the molecules as described in Sec. III B. For all five nuclear DOF included, a harmonic oscillator discrete variable representation (DVR) of frequency and mass 1.0 a.u. was employed. Description of the number of primitive basis functions and single particle functions is given in Table I.

TABLE I. Number of single particle functions for each nuclear DOF and electronic state and size of the DVR grid for each nuclear DOF for cyclobutanone/cyclopentanone.

DOF	Ground	(n, π^*)	$(n, 3s)$	$(n, 3p)$	DVR grid
ν_1/ν_1	1	8	4	3	60/60
ν_2/ν_3	1	8	4	3	55/55
ν_7/ν_8	1	8	4	3	80/60
ν_{12}/ν_{16}	1	8	4	3	100/100
ν_{21}/ν_{28}	1	8	4	3	170/170

The ground state wave function was obtained via energy relaxation by propagation in negative imaginary time $t = -i\tau$.[19,22] The initial wave packet in the $(n, 3s)$ state was taken to be the Franck-Condon wave packet obtained by operating with a unit dipole operator on the ground state wave function. This corresponds to exciting the system by an electric field of a time duration much shorter than the timescale for nuclear motion, which couples the ground and $(n, 3s)$ states. As the Condon approximation is invoked, any dependence of the transition dipole moment on the nuclear DOF, such as the linear Herzberg-Teller effect,[23] is neglected. This does not amount to a significant approximation as any difference in magnitude of the transition dipole moment over the ground state nuclear wave function is negligible as the wave function is very narrow. The system was subsequently propagated for 15 ps for cyclobutanone and 60 ps for cyclopentanone with a time step of 0.2 fs using the variable mean field integration scheme with a 6th order Adams-Bashforth-Moulton predictor-corrector integrator and an error tolerance of 10^{-8}.

B. The Hamiltonian

In the vibronic coupling scheme, the Hamiltonian (vibronic coupling Hamiltonian, VCHAM) is represented in a diabatic basis as an expansion around a point of interest $\boldsymbol{Q}_0$, chosen here to be the Franck-Condon point.[24–26] A general system of N electronic states is described by an $N \times N$ matrix, which is decomposed into a zero-order Hamiltonian $\boldsymbol{H}^{(0)}$ and a diabatic potential coupling matrix $\boldsymbol{W}$

$$\boldsymbol{H} = \boldsymbol{H}^{(0)} + \boldsymbol{W} = \sum_i \frac{\omega_i}{2} \left(Q_i^2 - \frac{\partial^2}{\partial Q_i^2} \right) \boldsymbol{I} + \boldsymbol{W}. \qquad (3)$$

Here, ω_i is the normal mode frequency, Q_i the position operator for nuclear DOF i, and $\boldsymbol{I}$ is the $N \times N$ identity matrix. The electronic on- and off-diagonal terms of $\boldsymbol{W}$ are, in this work, restricted to

$$W_{mm} = E^{(m)} + \sum_i \kappa_i^{(m)} Q_i + \frac{1}{2} \sum_{ij} \gamma_{ij}^{(m)} Q_i Q_j$$
$$+ \frac{1}{6} \sum_{ij} \iota_{ij}^{(m)} Q_i Q_j^2 + \frac{1}{24} \sum_i \epsilon_i^{(m)} Q_i^4, \qquad (4)$$

$$W_{ml} = \sum_i \lambda_i^{(m,l)} Q_i + \frac{1}{2} \sum_{ij} \mu_{ij}^{(m,l)} Q_i Q_j$$
$$+ \frac{1}{6} \sum_{ij} \eta_{ij}^{(m,l)} Q_i Q_j^2. \qquad (5)$$

The on-diagonal quartic terms are necessary in order to adequately describe the anharmonic low frequency DOF ν_1 and ν_2/ν_3. The cubic terms are included in order to describe anharmonicity, in particular in the coupling between nuclear DOF. A similar expansion has previously been used to describe benzene.[27] In cases of very anharmonic nuclear DOF, ν_{21} for cyclobutanone and ν_{28} for cyclopentanone, it was useful to employ a Morse potential as the zero order term (instead

of the harmonic term)

$$V_i^{(m)} = D_{i0}^{(m)} \left[\exp(-\alpha_i^{(m)}(Q_i - Q_{i0}^{(m)})) - 1 \right]^2 . \quad (6)$$

The product form of the VCHAM is necessary for the efficient evaluation of matrix elements in the MCTDH scheme and has therefore been combined with this several times before.[27–35] The parameters of the VCHAM, i.e., $\kappa_i^{(m)}$, $\epsilon_i^{(m)}$ etc.,[36] were fitted to *ab initio* data using a locally modified version of the VCHFIT program, which is distributed with the Heidelberg MCTDH code. An exponential weighting function $w_m = \exp(-\beta[E_m(\mathbf{Q}) - E_m(\mathbf{Q}_0)])$ was employed, where E_m is the *ab initio* energy of state m, and β is a factor taken to be 0.5 except for the excited states of cyclobutanone, where it was taken to be 1.0. This exponential weighting favors a good fit to the important low-energy regions of the surfaces. A Powell second-order optimization scheme was employed, which uses the mean-square difference between fit and data at all points as a penalty function. The *ab initio* data consisted of 1182 points for cyclobutanone and 1273 points for cyclopentanone, and the ground state was assumed uncoupled from the excited states.

C. Electronic structure

The ground state equilibrium structure of cyclobutanone and cyclopentanone was obtained at the MP2/cc-pVTZ (Ref. 37) and the CCSD/cc-pVTZ level of theory in GAUSSIAN 03 (Ref. 38). Coupled-cluster calculations of the excited states, at the CC2,[39] CCSD,[40,41] and CCSDR(3) (Refs. 42 and 43) level were performed using either the linear-response (LR) formalism in the Dalton Quantum Chemistry Program 2.0 (Ref. 44) or the equation of motion (EOM) formalism in CFOUR.[45] The equilibrium structures of the (n, π^*) and $(n, 3s)$ states were obtained using EOM coupled-cluster singles and doubles (EOM-CCSD) (Refs. 46–48) in CFOUR. For all coupled-cluster calculations, the core orbitals were frozen and a cc-pVTZ basis set was employed. The basis set was augmented by a set of 1s1p1d diffuse functions optimally contracted for each molecule from a primitive set of 8s8p8d according to the prescription in Ref. 49 to describe the diffuse Rydberg states.[36]

III. RESULTS AND DISCUSSION

A. Excited states of the cycloketones

The lowest excited state of cyclobutanone and cyclopentanone results from an $n \rightarrow \pi^*$ transition. For cyclobutanone, the band maximum of this transition is observed at 4.41 eV in *n*-hexane,[50] while it is slightly blue-shifted to 4.44 eV in the vapor phase.[51] For cyclopentanone, the band maximum is observed at 4.13 eV in *n*-hexane,[50] while the vertical transition energy has been determined from electron ionization to be 4.2 eV.[52] Table II presents the vertical transition energies to the (n, π^*) state as well as the $(n, 3s)$ and $(n, 3p)$ states calculated using three coupled-cluster methods. For the (n, π^*) state, the calculated excitation energies slightly decrease from CC2 to CCSD and to CCSDR(3). Although all values

TABLE II. Symmetry of and vertical excitation energy to (in eV) the (n, π^*) valence and $(n, 3s)$ and $(n, 3p)$ Rydberg states of cyclobutanone/cyclopentanone calculated using linear response CC2, CCSD, and CCSDR(3) with a cc-pVTZ+1s1p1d basis set.

State	Symmetry	CC2	CCSD	CCSDR(3)
(n, π^*)	A″/A	4.48/4.53	4.45/4.36	4.41/4.31
$(n, 3s)$	A″/B	6.02/5.85	6.60/6.48	6.50/6.37
$(n, 3p_x)$	A″/A	6.56/6.36	7.17/7.00	7.07/6.91
$(n, 3p_z)$	A″/B	6.69/6.51	7.28/7.16	7.18/7.05
$(n, 3p_y)$	A′/A	6.71/6.52	7.34/7.19	7.23/7.08

are in fair agreement with the experimental values, a large improvement is observed at the CCSD level of theory compared to CC2 in the case of cyclopentanone contrary to what has previously been found for valence states in recent benchmark studies.[53–55]

The structured $(n, 3s)$ absorption band of vapor phase cyclobutanone has a band maximum at ∼6.4 eV, while the origin is at 6.11 eV.[56,57] For cyclopentanone, the origin and band maximum from absorption coincide at 6.21 eV,[57] which is consistent with high-level REMPI experiments,[58,59] however, electron ionization locates the vertical transition energy slightly higher at 6.3 eV.[52] The origin of the lowest 3p Rydberg state in cyclobutanone is found at 6.94 eV, while the position of the band maximum at ∼7.2 eV is rather uncertain due to the nearby, strong 3d absorption band.[57] For cyclopentanone, the band maximum and origin again coincide at 6.95 eV, however, the vertical transition energy from electron ionization is again slightly higher at 7.2 eV.[52] Comparing to the calculated energies, the CC2 values are generally too low for the Rydberg states as seen also for other systems,[60] which is somewhat overcompensated for by CCSD. It can be observed that CCSDR(3) makes a small counter-correction of around 0.1 eV to the CCSD values. Generally, the CC2 energies are unsatisfactorily off from the experimental values, whereas the higher order methods perform better. There is of course some uncertainty when determining vertical transition energies from experiment, as these are not necessarily equivalent to the position of the band maximum,[61] but the latter conclusion is expected to hold nonetheless. As a significant number of calculations are needed for obtaining the data used for fitting the VCHAM, computational demands exclude the use of methods beyond CCSD. As CCSD also gives satisfactory results with errors <0.27 eV for the states considered, this method was used for all subsequent calculations.

As a final consideration, the dependence of the calculated excitation energies on the number of sets of diffuse functions was investigated. Up to three sets of diffuse functions were added to the cc-pVTZ basis set. The absolute change in transition energy to the (n, π^*) state was <2 meV, whereas it was <18 meV for the Rydberg states, thus, only one set of diffuse functions was deemed necessary.

B. The VCHAM

Due to the steep scaling of wave packet calculations on the number of DOF included in terms of computational demands, one inevitably has to make a decision on which
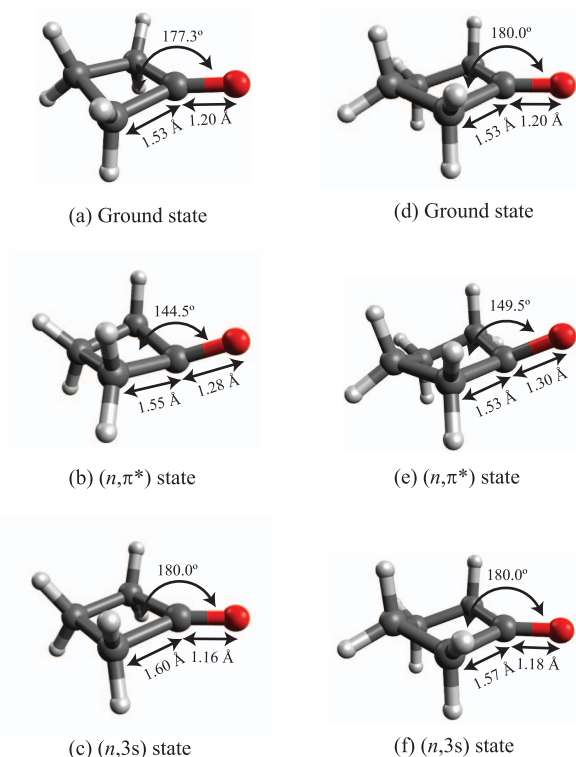
FIG. 1. Equilibrium structures of the (a)/(d) ground, (b)/(e) (n, π^*), and (c)/(f) $(n, 3s)$ states of cyclobutanone/cyclopentanone obtained at the CCSD/EOM-CCSD level of theory. Important geometrical differences are pointed out.

nuclear DOF to include and which to exclude in the description of the system. From the equilibrium structures of the ground, (n, π^*), and $(n, 3s)$ states, important information as to which geometrical changes that have to be described by the included nuclear DOF can be gained (see Fig. 1).

The C_s ground state structure of cyclobutanone is observed to be a slightly envelope puckered ring, with an almost 180° angle between the C=O-bond and the plane given by the carbonyl and the α-carbons (see Fig. 1(a)). In the (n, π^*) state, the latter angle is reduced to 144.5° by the out-of-plane deformation of the oxygen and the length of the C=O-bond is increased as expected due to population of the anti-bonding π^*-orbital (see Fig. 1(b)). Furthermore, the C−C-bonds adjacent to the carbonyl group are also lengthened due to the removal of the electron from the oxygen lone-pair orbital, which mixes with the σ-orbitals of the C−C-bonds. In the $(n, 3s)$ state, the four-membered ring is completely flat and the C−C-bond lengths are further increased, whereas the C=O-length

is decreased (see Fig. 1(c)). As the vibronic coupling Hamiltonian is given in terms of dimensionless normal mode coordinates, it is evidently important to include the carbonyl stretch to describe the changing C=O-bond length, ring-puckering and carbonyl out-of-plane deformation to describe the changing ring-structure and C=O bond to C−C−C plane angle as well as ring modes affecting the length of the C−C-bonds.

The C_2 ground state structure of cyclopentanone is a puckered ring (see Fig. 1(d)). Similar differences are observed between the equilibrium structures of the ground state and the two excited states, as for cyclobutanone except for the flattening of the ring in the Rydberg state (see Figs. 1(d)–1(e)). On the basis of these observed structural differences, we include in our VCHAM five nuclear DOF, three ring-modes (ring-pucker, and symmetric and asymmetric C−CO−C stretch), as well as two carbonyl modes (carbonyl stretch and out-of-plane deformation) (see Table III).

The normal mode coordinates as well as the zero order harmonic potential of the VCHAM are defined from the MP2/cc-pVTZ frequencies given in Table III along with a comparison to experimental values. The calculated values are slightly higher than the experimental, which can be expected from MP2.

Cuts through the potential energy surfaces showing both the *ab initio* points as well as the fits can be seen in Figs. 2 and 3. The adequacy of the fit to the *ab initio* points can be quantified by the root-mean square deviation (RMSD). For the fit to the ground states, the RMSD is 5.0 meV for cyclobutanone and 13.9 meV for cyclopentanone. For the excited states, the RMSD is 8.2 meV and 4.3 meV, respectively. In the calculation of the RMSD, the exponential weighting factor is taken into account.

C. The dynamical nature of the $(n, \pi^*) \leftarrow (n, 3s)$ transition

1. Symmetry considerations

Although very similar, cyclobutanone and cyclopentanone do represent two distinct systems primarily due to their differing point group symmetry at the Franck-Condon geometry.

For cyclobutanone, which belongs to the C_s point group, both the $(n, 3s)$ and the (n, π^*) state transform according to the A'' irreducible representation (see Table II). For a given matrix element $\langle \psi_l | W | \psi_m \rangle$ in Fermi's golden rule expression of Eq. (1) not to be zero on grounds of symmetry, we must

TABLE III. Calculated harmonic frequencies and experimental frequencies in [cm^{-1}] for the five nuclear DOF included in the VCHAM along with their symmetry and description for cyclobutanone/cyclopentanone.

Nuclear DOF	Symmetry	MP2/cc-pVTZ	Experimental[62,63]	Description
ν_1/ν_1	A′/B	114/97	~50/95	Ring-pucker
ν_2/ν_3	A′/B	404/452	395/446	C=O out-of-plane deformation
ν_7/ν_8	A′/A	889/837	850/804	Symmetric C−CO−C stretch
ν_{12}/ν_{16}	A″/B	1107/1188	956/1142	Asymmetric C−CO−C stretch
ν_{21}/ν_{28}	A′/A	1855/1808	1816/1770	C=O stretch

FIG. 2. Cyclobutanone: Examples of *ab initio* data (points) and VCHAM fits (lines) along ν_1 and ν_2 and along the diagonals $\nu_7\nu_{12}$ and $\nu_1\nu_{21}$.

have

$$\Gamma_m \otimes \Gamma_W \otimes \Gamma_l \supset A , \qquad (7)$$

where Γ label an irreducible representation, m and l label the electronic states, and A is the totally symmetric representation of the pertinent point group. In the VCHAM, the symmetry of W depends on the nuclear DOF involved, and we can rewrite the above equation to

$$\Gamma_m \otimes \left(\prod_{i}^{\text{order}} \Gamma_i \right) \otimes \Gamma_l \supset A . \qquad (8)$$

Here, the product runs over the number of coordinates involved in the coupling labeled by i, which is implied by the order of the coupling. For couplings linear in the given nuclear DOF ν_i, we must then have $\Gamma_i = A'$ for cyclobutanone. It is thus the totally symmetric, Franck-Condon active nuclear DOF that linearly couple the two states, and this coupling is present from the moment of excitation of the system. Four such DOF are included in the VCHAM; ν_1, ν_2, ν_7, and ν_{21} (see Table III). From the VCHAM, the largest linear interstate coupling coefficient $\lambda_i^{(m,l)}$ is found for ν_2 at 0.23 eV, which

is three times larger than the linear coupling of ν_1 and ν_{21} and an order of magnitude larger than that of ν_7. The linear coupling accounts for the largest part of the interstate coupling as the second and third order interstate coupling coefficients $\mu_{ij}^{(m,l)}$ and $\eta_{ij}^{(m,l)}$ are one and two orders of magnitude, respectively, smaller than the largest linear coupling coefficient.

In cyclopentanone, which belongs to the C_2 point group, the $(n, 3s)$ state transforms according to the B irreducible representation, whereas the (n, π^*) state transforms according to A. Thus, in contrast to what is found for cyclobutanone, it is the non-Franck-Condon active nuclear DOF transforming according to B, which couple the two states linearly. Three such DOF are included in the VCHAM; ν_1, ν_3, and ν_{16} (see Table III). These nuclear DOF are not activated upon excitation unless the Herzberg-Teller effect or a higher order dependence of the transition dipole moment on the nuclear DOF is significant. However, the change of the electronic transition dipole moment in a distance of $\langle \delta Q_i \rangle = \sqrt{\langle Q_i^2 \rangle - \langle Q_i \rangle^2}$ from the center of the ground state wave function is in these DOF <1.2% as calculated by LR-CCSD, thereby, confirming the
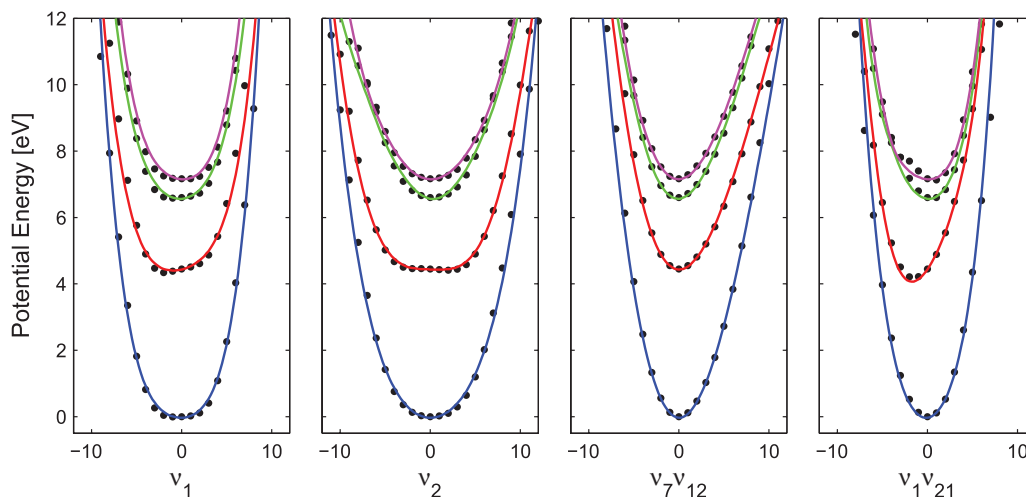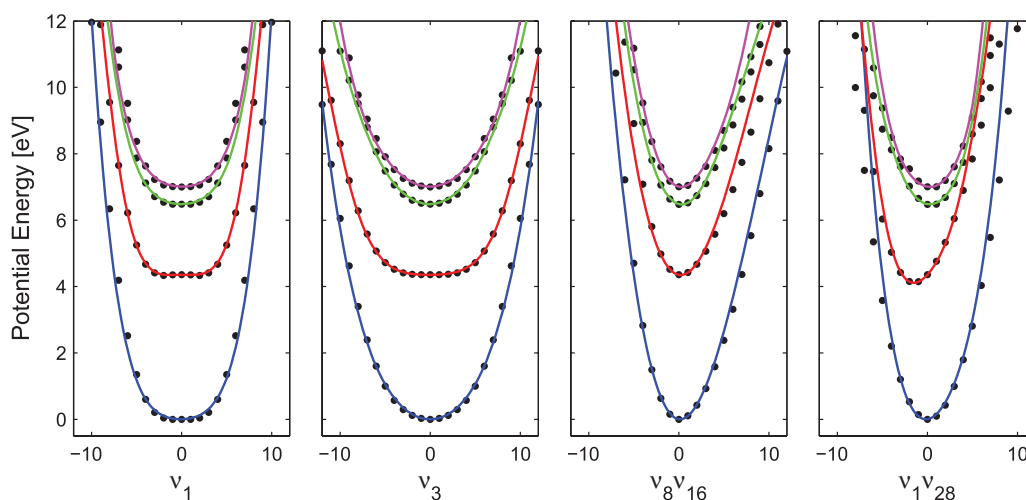

FIG. 3. Cyclopentanone: Examples of *ab initio* data (points) and VCHAM fits (lines) along ν_1 and ν_3 and along the diagonals $\nu_8\nu_{16}$ and $\nu_1\nu_{28}$.

validity of the employed Condon approximation. Due to the spread of the wave packet, however, the linear interstate couplings are not zero, and these initially only vary as the wave packet potentially spreads and contracts while the expectation value remains the same. On a longer time scale, internal vibrational energy redistribution (IVR) through coupling of the nuclear DOF within a given electronic state leads to the activation of these DOF and the population can better be "funneled away" on the lower surface. The leading terms accounting for IVR between A and B nuclear DOF are the third order intrastate couplings. The largest third order intrastate coupling coefficients $\iota_{ij}^{(m)}$ are found for the coupling between ν_{28} and ν_1 at -0.01 eV and ν_8 and ν_1 at 0.01 eV, while the coupling between ν_8 and ν_{16} is slightly smaller. Linear coupling coefficients $\lambda_i^{(m,l)}$ on the same order of magnitude as those for cyclobutanone are found for ν_1, ν_3, and ν_{16} of 0.16 eV, -0.08 eV, and -0.22 eV, respectively. The second and third order interstate coupling coefficients $\mu_{ij}^{(m,l)}$ and $\eta_{ij}^{(m,l)}$ are at least one and two orders of magnitude smaller, respectively. One exception is the third order coupling coefficient, which is cubic in ν_{16} of 0.01 eV.

2. The timescale of population transfer

From the above symmetry considerations, it is apparent that a significantly slower transition between the $(n, 3s)$ state and the (n, π^*) state can be expected for cyclopentanone. Although the linear coupling coefficients of the two molecules are of the same order of magnitude, IVR is a serious bottleneck for activating the reactive coupling nuclear DOF in cyclopentanone as this does not occur until the third order.

Figure 4 depicts the population of the three excited states as a function of time following excitation. A clear difference of time scale for the two molecules is apparent. The decay of the $(n, 3s)$ state for cyclobutanone exhibits biexponential behavior and can be adequately fitted with time constants of 0.95 ps and and 6.32 ps, whereas a similar fit to the $(n, 3s)$ population of cyclopentanone yields time constants of 3.62 ps and 58.1 ps.[64] Furthermore, the ratio of the amplitude of the short component to that of the long component is 5.5 times as large for cyclobutanone compared to cyclopentanone suggesting a difference of importance of the processes giving rise to these two features for the two molecules. The two short time constants are very close to the ones determined experimentally using TR-MS and TR-PES,[17] with the largest discrepancy found for cyclopentanone, where it is a factor of ~ 1.5 off. A perhaps more reasonable comparison to the experimental data is based on only fitting a single exponential decay to the populations, by which we find the time constants 2.05 and 22.2 ps for cyclobutanone and cyclopentanone, respectively. The ratio of these time scales are $\sim 1{:}11$, which is in the vicinity of the ratio of 2:13 found experimentally. However, as the population decay is not a direct measure of the decay of the ion or photoelectron yield, a full simulation of the time-resolved spectra would be necessary in order to determine if the current model fully explains all the features of the experimental signal.
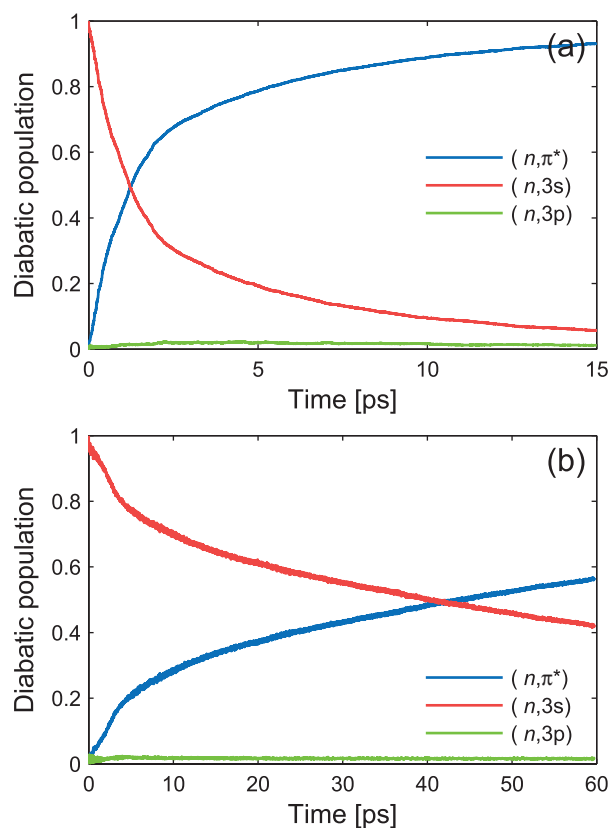
FIG. 4. Diabatic populations for the three excited states of (a) cyclobutanone and (b) cyclopentanone following excitation to the $(n, 3s)$ state.

3. Deconstructing the timescales: Vibronic coupling and internal vibrational energy redistribution

The linear interstate couplings $\lambda_i^{(2,3)} Q_i$ with $i = 2, 21$ for cyclobutanone, see Fig. 5(a), account for $\sim 90\%$ of the total coupling matrix element $\langle n, \pi^* | W | n, 3s \rangle$, and as expected, the coupling involving ν_2 gives the largest contribution. In the first 1 ps, the intrastate coupling between ν_2 and ν_{21} leads to an oscillatory modulation of the linear couplings involving these nuclear DOF. The frequency of this modulation corresponds for both to the frequency of ν_2 in the $(n, 3s)$ state, and it is observed to be π-phase shifted between the two linear couplings. After the first couple of ps, no significant changes are observed in the linear couplings.

Figure 5(b) shows the Fourier-transform of the total interstate coupling for the first 5 ps and the subsequent 10 ps of the propagation. In the short time spectrum, peaks are observed at ~ 269, ~ 607, ~ 855, and ~ 1535 cm^{-1}, which from the Fourier-transform of the coordinate expectation values can be seen, as expected, to correspond to motion in ν_1, ν_2, ν_7, and ν_{21}, respectively, on the $(n, 3s)$ state. In the longer time spectrum, the peak corresponding to motion in ν_1 on the $(n, 3s)$ state disappears, however, the peak at ~ 380 cm^{-1} corresponds to motion in the same nuclear DOF but on the (n, π^*) state such that the coupling is to a larger degree controlled by the dynamics on the lower surface as expected due to the population transfer. Furthermore, a progression is observed starting at ~ 1275 cm^{-1} spaced by ~ 400 cm^{-1}, which must be due to higher order couplings involving several nuclear DOF.
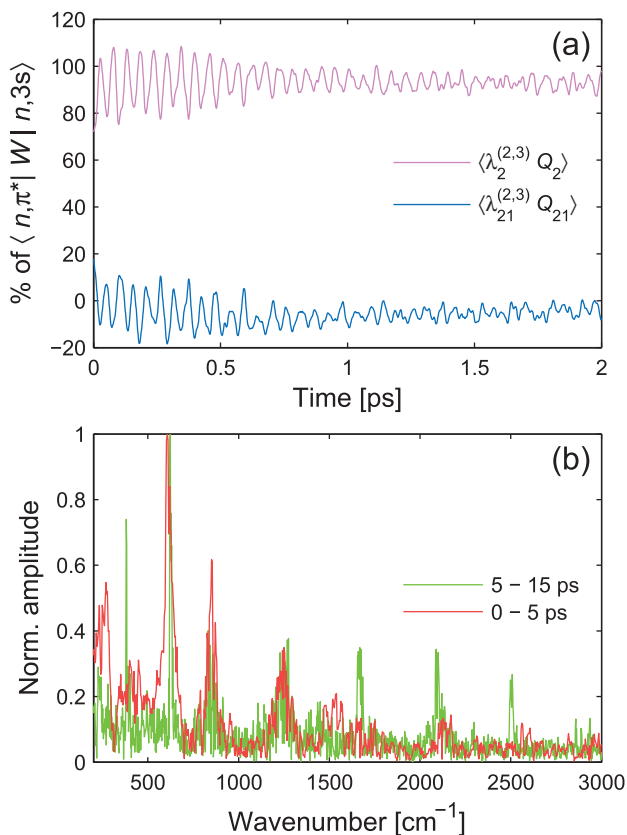
FIG. 5. Cyclobutanone: (a) Linear couplings $\lambda^{(2,3)}$ between the $(n, \pi*)$ and $(n, 3s)$ states in percentage of the total coupling between these two states, and (b) Fourier transform of the first 5 ps of the total coupling (red) and of the following 10 ps from 5 to 15 ps (green).

FIG. 6. Cyclopentanone: (a) Linear couplings $\lambda^{(2,3)}$ between the $(n, \pi*)$ and $(n, 3s)$ states in percentage of the total coupling between these two states, and (b) Fourier transform of the first 5 ps of the total coupling (red) and of the following 20 ps from 5 to 25 ps (green).

For cyclopentanone, the linear interstate couplings $\lambda_i^{(2,3)} Q_i$ with $i = 1, 3, 16$ account for ~105% of the total coupling matrix element $\langle n, \pi*|W|n, 3s \rangle$ (see Fig. 6(a)). Thus, some higher order couplings must be of opposite sign. As expected on the basis of the size of the coefficients, the largest coupling is found for ν_{16}.

Figure 6(b) shows the Fourier-transform of the total interstate coupling for the first 5 ps and the subsequent 20 ps of the propagation. For both time periods, the largest amplitude component is found with a frequency ~2070 cm^{-1}, which corresponds to the frequency of the standard deviation of the position operator for ν_{16} given by $\langle \delta Q_i \rangle = \sqrt{\langle Q_i^2 \rangle - \langle Q_i \rangle^2}$. It is thus the spreading and contracting motion of the wave packet in ν_{16}, which leads to the largest modulation of the interstate coupling. In the short time spectrum, peaks are also observed at ~1220 and ~1530 cm^{-1}, which are related to couplings involving ν_{16} in combination with ν_1 and ν_3, respectively. In the long time spectrum, peaks which can be directly associated with spreading and contracting motion in ν_1 and ν_3 are observed at ~420 cm^{-1} and ~1060 cm^{-1}. The peak ~1150 cm^{-1} is most likely due to a bilinear coupling involving ν_1 and ν_{28}, whereas the peak at ~1510 cm^{-1} is due to a third order coupling involving ν_3 and ν_{16}.

Two time scales were deduced for the population transfer for cyclopentanone, and it is also apparent that there is a slight shift of which DOF are most important in modulat-

ing the interstate coupling. At first, the modulation is mostly due to ν_{16}, whereas at later times, the lower frequency nuclear DOF also play a role. The amplitude of the oscillation of the expectation value of the position operator for the different nuclear DOF also exhibits two time scales (see Fig. 7). Over the first 5–10 ps, a significant degree of IVR is observed as energy is transferred from the initially activated ν_8 and ν_{28} to the three coupling DOF. It is also observed that the amplitude
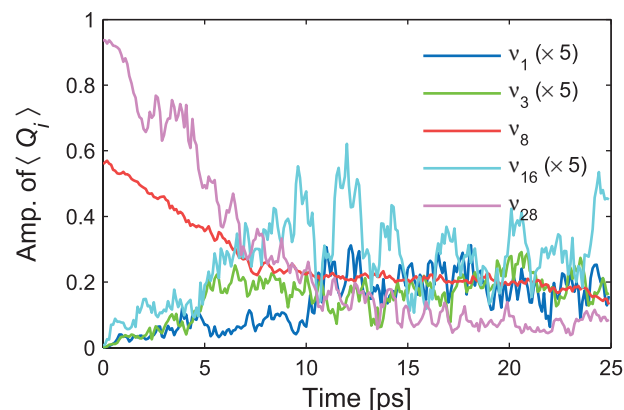
FIG. 7. Cyclopentanone: Amplitude of the oscillation of the expectation value of the position operator in the $(n, 3s)$ state for the five nuclear DOF as a function of time. Notice that the amplitudes for ν_1, ν_3, and ν_{16} have been multiplied by a factor of 5.

is around two times larger for ν_{16} compared to ν_1 and ν_3 in this time period except for a small window around 5 ps. On a longer time scale, on the other hand, we observe a somewhat constant amplitudes of motion for all nuclear DOF somewhat resembling the equidistribution of energy among the nuclear DOF. Thus, on the shorter time scale, motion in ν_{16} is to a large degree responsible for the coupling and the modulation of the coupling between the two electronic states, whereas at later times low frequency motion in ν_1 and ν_3 also partake.

IV. CONCLUSION

On the basis of *ab inito* data at the CCSD level of theory, we constructed five-dimensional vibronic coupling Hamiltonians (VCHAM) for the four lowest singlet electronic states of cyclobutanone and cyclopentanone. The five nuclear degrees of freedom (DOF) were chosen on the basis that they should be able to describe the significant structural changes between the equilibrium geometries of the ground, (n, π^*), and $(n, 3s)$ states. The VCHAM were subsequently used in wave packet calculations to investigate the nature of the $(n, \pi^*) \leftarrow (n, 3s)$ internal conversion.

In cyclobutanone, the population transfer from the $(n, 3s)$ state to the (n, π^*) state exhibits biexponential behavior with time constants 0.95 ps and and 6.32 ps. The coupling is mainly due to motion in the Franck-Condon active ν_2, the C=O out-of-plane deformation, however, motion in ν_1, the ring-puckering, also makes a significant contribution.

In cyclopentanone, a biexponential population decay is also observed with time constants of 3.62 ps and 58.1 ps. Initially, the interstate coupling is mainly modulated due to the spreading and contracting motion of the wave packet in ν_{16}, the asymmetric C−CO−C stretch. As internal vibrational energy redistribution (IVR) transfers energy from the initially excited ν_8 and ν_{28}, the symmetric C−CO−C and carbonyl stretch, respectively, the lower frequency motion in ν_1 and ν_3, the ring-puckering and the C=O out-of-plane deformation, respectively, start to play a larger role in the interstate coupling.

The time scales determined from the single exponential fits to the $(n, 3s)$ population decay of the two molecules exhibit a 1:11 ratio somewhat similar to the 2:13 ratio determined from experiment.[17] This difference of time scales covers two significantly different dynamical pictures, which to a large degree hinges on the differing electronic state symmetries found in the two molecules: one direct population transfer and one indirect.

In cyclobutanone, the direct picture is prominent, as seen by the large amplitude of the short component of the biexponential fit to the $(n, 3s)$ population decay, which results from the direct motion in the reactive nuclear DOF. For cyclopentanone, this short component has a much smaller amplitude as the reactive nuclear DOF are not activated initially. The indirect picture is most prominent in cyclopentanone. In this picture, the energy is deposited in non-reactive DOF and IVR is necessary and represents a bottleneck for mediating the transfer of energy to the reactive nuclear DOF on a $\sim$5–10 ps time scale, whereafter population transfer proceeds. Whence, as observed, the complex nature of internal conversion ne-

cessitates full dynamics simulations to infer such qualitative pictures as presented herein.

[1] E. W.-G. Diau, J. L. Herek, Z. H. Kim, and A. H. Zewail, Science **279**, 847 (1998).
[2] K. B. Møller and A. H. Zewail, *Essays in Contemporary Chemistry: From Molecular Structure Towards Biology* (Wiley VCH, Zürich, 2001), Chap. 5, pp. 157–188.
[3] B. G. Levine and T. J. Martinez, Annu. Rev. Phys. Chem. **58**, 613 (2007).
[4] T. S. Kuhlman, W. J. Glover, T. Mori, K. B. Møller, and T. J. Martinez, "Between ethylene and polyenes—The non-adiabatic dynamics of *cis*-dienes," Faraday Discuss. (in press).
[5] D. R. Yarkony, Rev. Mod. Phys. **68**, 985 (1996).
[6] D. R. Yarkony, J. Phys. Chem. A **105**, 6277 (2001).
[7] T. J. Martinez, Nature (London) **467**, 412 (2010).
[8] R. A. Marcus, J. Chem. Phys. **20**, 359 (1952).
[9] N. J. Turro, J. C. Scaiano, and V. Ramamurthy, *Modern Molecular Photochemistry of Organic Molecules* (University Science Books, Sausalito, California, 2010), pp. 328–341.
[10] D. J. Tannor, *Introduction to Quantum Mechanics—A Time-Dependent Perspective* (University Science Books, Sausalito, CA, 2007), p. 438.
[11] S. Pedersen, J. L. Herek, and A. H. Zewail, Science **266**, 1359 (1994).
[12] E. W. G. Diau, C. Kötting, and A. H. Zewail, ChemPhysChem **2**, 273 (2001).
[13] E. W. G. Diau, C. Kötting, and A. H. Zewail, ChemPhysChem **2**, 294 (2001).
[14] A. P. Baronavski and J. C. Owrutsky, Chem. Phys. Lett. **333**, 36 (2001).
[15] E. W.-G. Diau, C. Kötting, T. I. Sølling, and A. H. Zewail, ChemPhysChem **3**, 57 (2002).
[16] T. I. Sølling, E. W.-G. Diau, C. Kötting, S. De Feyter, and A. H. Zewail, ChemPhysChem **3**, 79 (2002).
[17] T. S. Kuhlman, T. I. Sølling, and K. B. Møller, ChemPhysChem **13**, 820 (2012).
[18] H.-D. Meyer, U. Manthe, and L. S. Cederbaum, Chem. Phys. Lett. **165**, 73 (1990).
[19] M. H. Beck, A. Jäckle, G. A. Worth, and H.-D. Meyer, Phys. Rep. **324**, 1 (2000).
[20] G. Worth, F. Gatti, and H.-D. Meyer, *Multi-dimensional Quantum Dynamics* (Wiley, 2009).
[21] G. A. Worth, M. H. Beck, A. Jäckle, and H.-D. Meyer, The MCTDH Package, Version 8.2, (2000); H.-D. Meyer, Version 8.3 (2002), Version 8.4 (2007); see http://mctdh.uni-hd.de.
[22] R. Kosloff and H. Tal-Ezer, Chem. Phys. Lett. **127**, 223 (1986).
[23] G. Herzberg and E. Teller, Z. Phys. Chem. Abt. B **21**, 410 (1933).
[24] L. S. Cederbaum, W. Domcke, H. Köppel, and W. von Niessen, Chem. Phys. **26**, 169 (1977).
[25] L. S. Cederbaum, H. Köppel, and W. Domcke, Int. J. Quantum Chem. **20**, 251 (1981).
[26] H. Köppel, W. Domcke, and L. S. Cederbaum, *Multimode Molecular Dynamics Beyond the Born-Oppenheimer Approximation*, Advances in Chemical Physics (Wiley, New York, 1984), Vol. 57, pp. 59–246.
[27] T. J. Penfold and G. A. Worth, J. Chem. Phys. **131**, 064303 (2009).
[28] G. A. Worth, H.-D. Meyer, and L. S. Cederbaum, J. Chem. Phys. **105**, 4412 (1996).
[29] G. A. Worth, H.-D. Meyer, and L. S. Cederbaum, J. Chem. Phys. **109**, 3518 (1998).
[30] G. A. Worth, H.-D. Meyer, and L. S. Cederbaum, Chem. Phys. Lett. **299**, 451 (1999).
[31] A. Raab, G. A. Worth, H.-D. Meyer, and L. S. Cederbaum, J. Chem. Phys. **110**, 936 (1999).
[32] S. Mahapatra, G. A. Worth, H.-D. Meyer, L. S. Cederbaum, and H. Köppel, J. Phys. Chem. A **105**, 5567 (2001).

[33]M. Doscher, H. Koppel, and P. G. Szalay, J. Chem. Phys. **117**, 2645 (2002).

[34]T. S. Venkatesan, S. Mahapatra, H.-D. Meyer, H. Koeppel, and L. S. Cederbaum, J. Phys. Chem. A **111**, 1746 (2007).

[35]G. A. Worth, R. E. Carley, and H. H. Fielding, Chem. Phys. **338**, 220 (2007).

[36]See supplementary material at http://dx.doi.org/10.1063/1.4742313 for complete Refs. 38, 45, and 49, the fitted coefficients of the vibronic coupling Hamiltonian and the coefficients and exponents of the diffuse functions.

[37]T. H. Dunning, J. Chem. Phys. **90**, 1007 (1989).

[38]M. J. Frisch, G. W. Trucks, H. B. Schlegel *et al.*, GAUSSIAN 03, Revision E.01, Gaussian, Inc., Wallingford, CT, 2004.

[39]O. Christiansen, H. Koch, and P. Jorgensen, Chem. Phys. Lett. **243**, 409 (1995).

[40]D. Mukherjee and P. K. Mukherjee, Chem. Phys. **39**, 325 (1979).

[41]H. Koch and P. Jørgensen, J. Chem. Phys. **93**, 3333 (1990).

[42]O. Christiansen, H. Koch, and F. Jørgensen, J. Chem. Phys. **105**, 1451 (1996).

[43]O. Christiansen, H. Koch, P. Jørgensen, and J. Olsen, Chem. Phys. Lett. **256**, 185 (1996).

[44]Dalton, a molecular electronic structure program, Release 2.0 (2005), see http://www.kjemi.uio.no/software/dalton/dalton.html.

[45]J. F. Stanton *et al.*, CFOUR, a quantum chemical program package; for the current version, see http://www.cfour.de.

[46]H. Sekino and R. J. Bartlett, Int. J. Quantum Chem. **26**, 255 (1984).

[47]J. F. Stanton and R. J. Bartlett, J. Chem. Phys. **98**, 7029 (1993).

[48]D. C. Comeau and R. J. Bartlett, Chem. Phys. Lett. **207**, 414 (1993).

[49]B. O. Roos, K. Andersson, M. P. Fülscher, P.-Å. Malmqvist, L. Serrano-Andrés, K. Pierloot, and M. Merchán, Adv. Chem. Phys. **93**, 219 (2007).

[50]M. O'Sullivan and A. C. Testa, J. Phys. Chem. **77**, 1830 (1973).

[51]J. C. Hemminger, H. A. J. Carless, and E. K. C. Lee, J. Am. Chem. Soc. **95**, 682 (1973).

[52]K. Furuya, E. Yamamoto, Y. Jinbou, and T. Ogawa, J. Electron Spectrosc. Relat. Phenom. **73**, 59 (1995).

[53]M. Schreiber, M. R. J. Silva, S. P. A. Sauer, and W. Thiel, J. Chem. Phys. **128**, 134110 (2008).

[54]S. P. A. Sauer, M. Schreiber, M. R. Silva-Junior, and W. Thiel, J. Chem. Theory Comput. **5**, 555 (2009).

[55]M. R. Silva Jr., S. P. A. Sauer, M. Schreiber, and W. Thiel, Mol. Phys. **108**, 453 (2010).

[56]C. R. Drury-Lessard and D. C. Moule, J. Chem. Phys. **68**, 5392 (1978).

[57]L. O'Toole, P. Brint, C. Kosmidis, G. Boulakis, and P. Tsekeris, J. Chem. Soc. Faraday T. **87**, 3343 (1991).

[58]T. J. Cornish and T. Baer, J. Am. Chem. Soc. **109**, 6915 (1987).

[59]A. R. Potts, D. R. Nesselrodt, T. Baer, J. W. Driscoll, and J. P. Bays, J. Phys. Chem. **99**, 12090 (1995).

[60]H. H. Falden, K. R. Falster-Hansen, K. L. Bak, S. Rettrup, and S. P. A. Sauer, J. Phys. Chem. A **113**, 11995 (2009).

[61]E. R. Davidson and A. A. Jarzecki, Chem. Phys. Lett. **285**, 155 (1998).

[62]K. Frei and H. H. Günthard, J. Mol. Spectrosc. **5**, 218 (1960).

[63]H. E. Howard-Lock and G. W. King, J. Mol. Spectrosc. **35**, 393 (1970).

[64]The time constant of 58.1 ps for cyclopentanone is connected with a large uncertainty as it is comparable to the total simulation time.

Supporting Information for:

Symmetry, Vibrational Energy Redistribution and Vibronic Coupling:

The Internal Conversion Processes of Cycloketones

Thomas S. Kuhlman,[1] Stephan P. A. Sauer,[2] Theis I. Sølling,[2] and Klaus B. Møller[1, a]

[1] *Department of Chemistry, Technical University of Denmark, Kemitorvet 207,*
DK-2800 Kgs. Lyngby, Denmark

[2] *Department of Chemistry, University of Copenhagen, Universitetsparken 5,*
DK-2100 København Ø, Denmark

(Dated: 20 July 2012)

---

[a] Electronic mail: klaus.moller@kemi.dtu.dk

CONTENTS

I.   COMPLETE REFERENCES

A.   Reference 38

M. J. Frisch, G. W. Trucks, H. B. Schlegel, G. E. Scuseria, M. A. Robb, J. R. Cheeseman, J. A. Montgomery, Jr., T. Vreven, K. N. Kudin, J. C. Burant, J. M. Millam, S. S. Iyengar, J. Tomasi, V. Barone, B. Mennucci, M. Cossi, G. Scalmani, N. Rega, G. A. Petersson, H. Nakatsuji, M. Hada, M. Ehara, K. Toyota, R. Fukuda, J. Hasegawa, M. Ishida, T. Nakajima, Y. Honda, O. Kitao, H. Nakai, M. Klene, X. Li, J. E. Knox, H. P. Hratchian, J. B. Cross, V. Bakken, C. Adamo, J. Jaramillo, R. Gomperts, R. E. Stratmann, O. Yazyev, A. J. Austin, R. Cammi, C. Pomelli, J. W. Ochterski, P. Y. Ayala, K. Morokuma, G. A. Voth, P. Salvador, J. J. Dannenberg, V. G. Zakrzewski, S. Dapprich, A. D. Daniels, M. C. Strain, O. Farkas, D. K. Malick, A. D. Rabuck, K. Raghavachari, J. B. Foresman, J. V. Ortiz, Q. Cui, A. G. Baboul, S. Clifford, J. Cioslowski, B. B. Stefanov, G. Liu, A. Liashenko, P. Piskorz, I. Komaromi, R. L. Martin, D. J. Fox, T. Keith, M. A. Al-Laham, C. Y. Peng, A. Nanayakkara, M. Challacombe, P. M. W. Gill, B. Johnson, W. Chen, M. W. Wong, C. Gonzalez, J. A. Pople, Gaussian 03, Revision E.01, Gaussian, Inc., Wallingford, CT, 2004.

B.   Reference 45

CFOUR, a quantum chemical program package written by J.F. Stanton, J. Gauss, M.E. Harding, P.G. Szalay with contributions from A.A. Auer, R.J. Bartlett, U. Benedikt, C. Berger, D.E. Bernholdt, Y.J. Bomble, L. Cheng, O. Christiansen, M. Heckert, O. Heun, C. Huber, T.-C. Jagau, D. Jonsson, J. Juslius, K. Klein, W.J. Lauderdale, D.A. Matthews, T. Metzroth, L.A. Mück, D.P. O'Neill, D.R. Price, E. Prochnow, C. Puzzarini, K. Ruud, F. Schiffmann, W. Schwalbach, S. Stopkowicz, A. Tajti, J. Vázquez, F. Wang, J.D. Watts and the integral packages MOLECULE (J. Almlöf and P.R. Taylor), PROPS (P.R. Taylor), ABACUS (T. Helgaker, H.J. Aa. Jensen, P. Jørgensen, and J. Olsen), and ECP routines by A. V. Mitin and C. van Wüllen. For the current version, see http://www.cfour.de.

C. Reference 49

B. O. Roos, K. Andersson, M. P. Fülscher, P.-Å. Malmqvist, L. Serrano-Andrés, K. Pierloot and M. Merchán,, Multiconfigurational Perturbation Theory: Applications in Electronic Spectroscopy, in *New Methods in Computational Quantum Mechanics*, volume 93 of *Adv. Chem. Phys.*, pages 219–331, John Wiley & Sons Inc., New York, 1996.

II. PARAMETERS OF THE VIBRONIC COUPLING HAMILTONIAN

The constants of the vibronic coupling Hamiltonian (VCHAM) obtained from fitting to adiabatic potential energy surfaces calculated at the EOM-CCSD/cc-pVTZ-1s1p1d level of theory are given in Tables I–X for cyclobutanone and XI–XX for cyclopentanone. Constants not given in the tables are either zero by symmetry, negligible or not included. The electronic labels $m, l \in \{1, 2, 3, 4\}$ corresponding to the ground, (n, π^*), $(n, 3\mathrm{s})$, and $(n, 3\mathrm{p})$ state respectively. The labels for the nuclear degrees of freedom $i, j \in \{1, 2, 7, 12, 21\}$ for cyclobutanone and $\{1, 3, 8, 16, 28\}$ for cyclopentanone.

A. Cyclobutanone

1. Electronic On-diagonal Parameters

TABLE I. Vibrational frequencies ω_i (in eV) for the normal modes of cyclobutanone.

Parameter	ν_1	ν_2	ν_7	ν_{12}	ν_{21}
ω_i	0.0141	0.0501	0.1102	0.1373	0.2300

TABLE II. On-diagonal constants $E^{(m)}$ (in eV) for the four states of cyclobutanone.

Parameter	1	2	3	4
$E^{(m)}$	0.0000	4.4654	6.5970	7.1847

4

TABLE III. Parameters of the Morse potential for ν_{21} for the four states of cyclobutanone.

Parameter	1	2	3	4
$D_{i0}^{(m)}$ [eV]	28.1696	19.4099	7.0043	4.5790
$\alpha_i^{(m)}$	-0.0651	-0.0657	-0.1029	-0.1167
$Q_{i0}^{(m)}$	-0.1140	-1.6670	0.3191	-0.0009
$E_0^{(m)}$ [eV]	-0.0016	-0.2598	-0.0073	0.0000

TABLE IV. On-diagonal linear coupling constants $\kappa_i^{(m)}$ (in eV) for the normal modes of cyclobutanone.

i	$\kappa_i^{(1)}$	$\kappa_i^{(2)}$	$\kappa_i^{(3)}$	$\kappa_i^{(4)}$
ν_1	0.0052	0.0653	0.0169	-0.0179
ν_2	-0.0027	-0.0074	-0.0453	-0.0096
ν_7	-0.0090	-0.0024	0.0189	0.0092
ν_{12}	$\cdots$	$\cdots$	$\cdots$	$\cdots$
ν_{21}	$\cdots$	$\cdots$	$\cdots$	$\cdots$

TABLE V. On-diagonal bilinear coupling constants $\gamma_{ij}^{(m)}$ (in eV) for the normal modes of cyclobutanone.

$\gamma_{ij}^{(1)}$	ν_1	ν_2	ν_7	ν_{12}	ν_{21}
ν_1	0.0744	-0.0094	-0.0057	$\cdots$	-0.0471
ν_2	-0.0094	0.0451	-0.0169	$\cdots$	-0.0493
ν_7	-0.0057	-0.0169	0.0092	$\cdots$	0.0134
ν_{12}	$\cdots$	$\cdots$	$\cdots$	0.0076	$\cdots$
ν_{21}	-0.0470	-0.0493	0.0134	$\cdots$	$\cdots$
$\gamma_{ij}^{(2)}$	ν_1	ν_2	ν_7	ν_{12}	ν_{21}
ν_1	0.0948	-0.0336	-0.0124	$\cdots$	-0.0639
ν_2	-0.0336	0.0115	-0.0203	$\cdots$	-0.0532
ν_7	-0.0124	-0.0203	0.0070	$\cdots$	0.0264
ν_{12}	$\cdots$	$\cdots$	$\cdots$	-0.0462	$\cdots$
ν_{21}	-0.0639	-0.0532	0.0264	$\cdots$	$\cdots$
$\gamma_{ij}^{(3)}$	ν_1	ν_2	ν_7	ν_{12}	ν_{21}
ν_1	0.0900	-0.0391	-0.0161	$\cdots$	-0.0308
ν_2	-0.0391	0.0478	-0.0192	$\cdots$	-0.0323
ν_7	-0.0161	-0.0192	0.0084	$\cdots$	0.0369
ν_{12}	$\cdots$	$\cdots$	$\cdots$	-0.0462	$\cdots$
ν_{21}	-0.0308	-0.0323	0.0369	$\cdots$	$\cdots$
$\gamma_{ij}^{(4)}$	ν_1	ν_2	ν_7	ν_{12}	ν_{21}
ν_1	0.0429	-0.0499	0.0081	$\cdots$	-0.0497
ν_2	-0.0499	0.0401	-0.0265	$\cdots$	-0.0467
ν_7	0.0081	-0.0265	-0.0264	$\cdots$	0.0253
ν_{12}	$\cdots$	$\cdots$	$\cdots$	-0.0492	$\cdots$
ν_{21}	-0.0497	-0.0467	0.0253	$\cdots$	$\cdots$

TABLE VI. On-diagonal linear-quadratic coupling constants $\iota_{ij}^{(m)}$ (in eV) for the normal modes of cyclobutanone.

$\iota_{ij}^{(1)}$	ν_1^2	ν_2^2	ν_7^2	ν_{12}^2	ν_{21}^2
ν_1	0.0085	$\cdots$	$\cdots$	$\cdots$	$\cdots$
ν_2	-0.0047	-0.0038	$\cdots$	0.0024	$\cdots$
ν_7	-0.0037	-0.0028	-0.0027	-0.0069	$\cdots$
ν_{12}	$\cdots$	$\cdots$	$\cdots$	$\cdots$	$\cdots$
ν_{21}	-0.0192	-0.0181	-0.0016	-0.0177	$\cdots$
$\iota_{ij}^{(2)}$	ν_1^2	ν_2^2	ν_7^2	ν_{12}^2	ν_{21}^2
ν_1	0.0004	0.0128	0.0082	-0.0011	0.0007
ν_2	-0.0126	0.0032	$\cdots$	0.0033	-0.0052
ν_7	-0.0108	-0.0001	-0.0031	-0.0079	-0.0007
ν_{12}	$\cdots$	$\cdots$	$\cdots$	$\cdots$	$\cdots$
ν_{21}	-0.0198	-0.0140	$\cdots$	-0.0220	-0.0016
$\iota_{ij}^{(3)}$	ν_1^2	ν_2^2	ν_7^2	ν_{12}^2	ν_{21}^2
ν_1	0.0095	0.0010	-0.0003	0.0001	0.0123
ν_2	-0.0062	0.0039	-0.0025	0.0020	-0.0025
ν_7	-0.0060	$\cdots$	-0.0029	-0.0076	-0.0009
ν_{12}	$\cdots$	$\cdots$	$\cdots$	$\cdots$	$\cdots$
ν_{21}	-0.0240	-0.0058	0.0012	-0.0174	-0.0025
$\iota_{ij}^{(4)}$	ν_1^2	ν_2^2	ν_7^2	ν_{12}^2	ν_{21}^2
ν_1	0.0039	0.0003	-0.0012	0.0019	0.0008
ν_2	-0.0016	-0.0008	$\cdots$	0.0003	-0.0116
ν_7	0.0024	0.0004	-0.0055	-0.0039	0.0001
ν_{12}	$\cdots$	$\cdots$	$\cdots$	$\cdots$	$\cdots$
ν_{21}	-0.0113	0.0022	0.0021	-0.0176	-0.0025

TABLE VII. On-diagonal quartic coupling constants $\epsilon_i^{(m)}$ (in eV) for the normal modes of cyclobutanone.

i	$\epsilon_i^{(1)}$	$\epsilon_i^{(2)}$	$\epsilon_i^{(3)}$	$\epsilon_i^{(4)}$
ν_1	0.0344	0.0308	0.0219	0.0315
ν_2	0.0082	0.0070	0.0018	0.0034
ν_7	0.0003	$\cdots$	-0.0015	0.0004
ν_{12}	0.0005	0.0017	0.0017	-0.0001
ν_{21}	$\cdots$	$\cdots$	$\cdots$	$\cdots$

2.   Electronic Off-diagonal Parameters

TABLE VIII. Off-diagonal linear coupling constants $\lambda_i^{(m,l)}$ (in eV) for the normal modes of cyclobutanone.

i	$\lambda_i^{(2,3)}$	$\lambda_i^{(2,4)}$	$\lambda_i^{(3,4)}$
ν_1	0.0693	0.2284	0.0024
ν_2	0.2251	0.1194	-0.0183
ν_7	-0.0287	-0.0678	-0.0448
ν_{12}	$\cdots$	$\cdots$	$\cdots$
ν_{21}	-0.0663	-0.0316	-0.0025

TABLE IX. Off-diagonal bilinear coupling constants $\mu_{ij}^{(m,l)}$ (in eV) for the normal modes of cyclobutanone.

$\mu_{ij}^{(2,3)}$	ν_1	ν_2	ν_7	ν_{12}	ν_{21}
ν_1	-0.0375	0.0342	0.0344	$\cdots$	0.0271
ν_2	0.0342	-0.0043	-0.0085	$\cdots$	0.0143
ν_7	0.0344	-0.0085	0.0025	$\cdots$	0.0148
ν_{12}	$\cdots$	$\cdots$	$\cdots$	-0.0007	$\cdots$
ν_{21}	0.0271	0.0143	0.0148	$\cdots$	-0.0154
$\mu_{ij}^{(2,4)}$	ν_1	ν_2	ν_7	ν_{12}	ν_{21}
ν_1	0.0116	-0.0019	-0.0090	$\cdots$	0.0009
ν_2	-0.0019	-0.0042	0.0051	$\cdots$	0.0092
ν_7	-0.0090	0.0051	0.0002	$\cdots$	-0.0010
ν_{12}	$\cdots$	$\cdots$	$\cdots$	-0.0023	$\cdots$
ν_{21}	0.0009	0.0092	-0.0010	$\cdots$	0.0038
$\mu_{ij}^{(3,4)}$	ν_1	ν_2	ν_7	ν_{12}	ν_{21}
ν_1	-0.0011	-0.0072	-0.0013	$\cdots$	-0.0056
ν_2	-0.0072	-0.0059	0.0033	$\cdots$	0.0082
ν_7	-0.0013	0.0033	-0.0008	$\cdots$	-0.0093
ν_{12}	$\cdots$	$\cdots$	$\cdots$	0.0008	$\cdots$
ν_{21}	-0.0056	0.0082	-0.0093	$\cdots$	0.0093

TABLE X. Off-diagonal linear-quadratic coupling constants $\eta_{ij}^{(m,l)}$ (in eV) for the normal modes of cyclobutanone.

$\eta_{ij}^{(2,3)}$	ν_1^2	ν_2^2	ν_7^2	ν_{12}^2	ν_{21}^2
ν_1	-0.0033	$\cdots$	$\cdots$	-0.0005	0.0001
ν_2	-0.0022	-0.0109	0.0021	-0.0007	$\cdots$
ν_7	-0.0018	-0.0025	0.0003	$\cdots$	0.0014
ν_{12}	$\cdots$	$\cdots$	$\cdots$	$\cdots$	$\cdots$
ν_{21}	0.0003	-0.0002	0.0025	0.0050	-0.0019
$\eta_{ij}^{(2,4)}$	ν_1^2	ν_2^2	ν_7^2	ν_{12}^2	ν_{21}^2
ν_1	-0.0113	$\cdots$	$\cdots$	-0.0014	$\cdots$
ν_2	-0.0072	-0.0081	$\cdots$	-0.0011	$\cdots$
ν_7	0.0026	0.0012	0.0027	-0.0005	$\cdots$
ν_{21}	$\cdots$	$\cdots$	$\cdots$	$\cdots$	$\cdots$
ν_{21}	-0.0073	-0.0023	0.0015	0.0002	0.0003
$\eta_{ij}^{(3,4)}$	ν_1^2	ν_2^2	ν_7^2	ν_{12}^2	ν_{21}^2
ν_1	0.0057	$\cdots$	$\cdots$	-0.0007	$\cdots$
ν_2	-0.0034	0.0033	$\cdots$	-0.0013	$\cdots$
ν_7	-0.0016	0.0009	0.0017		0.0001
ν_{12}	$\cdots$	$\cdots$	$\cdots$	$\cdots$	$\cdots$
ν_{21}	-0.0044	-0.0024	-0.0016	-0.0003	0.0008

B. Cyclopentanone

1. Electronic On-diagonal Parameters

TABLE XI. Vibrational frequencies ω_i (in eV) for the normal modes of cyclopentanone.

Parameter	ν_1	ν_3	ν_8	ν_{16}	ν_{28}
ω_i	0.0121	0.0561	0.1038	0.1473	0.2241

TABLE XII. On-diagonal constants $E^{(m)}$ (in eV) for the for the four states cyclopentanone.

Parameter	1	2	3	4
$E^{(m)}$	0.0000	4.3500	6.4804	7.0063

TABLE XIII. Parameters of the Morse potential for ν_{28} for the four states of cyclopentanone.

Parameter	1	2	3	4
$D_{i0}^{(m)}$ [eV]	40.8297	31.0856	6.7409	5.1947
$\alpha_i^{(m)}$	-0.0478	-0.0468	-0.0988	-0.1038
$Q_{i0}^{(m)}$	-0.1677	-1.9098	0.3899	0.4137
$E_0^{(m)}$ [eV]	-0.0026	-0.2718	-0.0096	-0.0092

TABLE XIV. On-diagonal linear coupling constants $\kappa_i^{(m)}$ (in eV) for the normal modes of cyclopentanone.

i	$\kappa_i^{(1)}$	$\kappa_i^{(2)}$	$\kappa_i^{(3)}$	$\kappa_i^{(4)}$
ν_1	$\cdots$	$\cdots$	$\cdots$	$\cdots$
ν_3	$\cdots$	$\cdots$	$\cdots$	$\cdots$
ν_8	-0.0288	-0.0445	-0.0543	-0.0543
ν_{16}	$\cdots$	$\cdots$	$\cdots$	$\cdots$
ν_{28}	$\cdots$	$\cdots$	$\cdots$	$\cdots$

TABLE XV. On-diagonal bilinear coupling constants $\gamma_{ij}^{(m)}$ (in eV) for the normal modes of cyclopentanone.

$\gamma_{ij}^{(1)}$	ν_1	ν_3	ν_8	ν_{16}	ν_{28}
ν_1	0.0350	0.0119	$\cdots$	0.0074	$\cdots$
ν_3	0.0119	0.0183	$\cdots$	-0.0108	$\cdots$
ν_8	$\cdots$	$\cdots$	0.0175	$\cdots$	0.0067
ν_{16}	0.0074	-0.0109	$\cdots$	0.0103	$\cdots$
ν_{28}	$\cdots$	$\cdots$	0.0067	$\cdots$	$\cdots$
$\gamma_{ij}^{(2)}$	ν_1	ν_3	ν_8	ν_{16}	ν_{28}
ν_1	0.0049	-0.0214	$\cdots$	-0.0247	$\cdots$
ν_3	-0.0214	-0.0372	$\cdots$	0.0196	$\cdots$
ν_8	$\cdots$	$\cdots$	0.0196	$\cdots$	0.0034
ν_{16}	-0.0247	0.0196	$\cdots$	0.0242	$\cdots$
ν_{28}	$\cdots$	$\cdots$	0.0034	$\cdots$	$\cdots$
$\gamma_{ij}^{(3)}$	ν_1	ν_3	ν_8	ν_{16}	ν_{28}
ν_1	0.0447	0.0109	$\cdots$	0.0185	$\cdots$
ν_3	0.0109	0.0139	$\cdots$	-0.0107	$\cdots$
ν_8	$\cdots$	$\cdots$	0.0046	$\cdots$	-0.0054
ν_{16}	0.0185	-0.0107	$\cdots$	-0.0713	$\cdots$
ν_{28}	$\cdots$	$\cdots$	-0.0054	$\cdots$	$\cdots$
$\gamma_{ij}^{(4)}$	ν_1	ν_3	ν_8	ν_{16}	ν_{28}
ν_1	0.0101	0.0135	$\cdots$	0.0189	$\cdots$
ν_3	0.0135	0.0123	$\cdots$	-0.0053	$\cdots$
ν_8	$\cdots$	$\cdots$	-0.0012	$\cdots$	-0.0047
ν_{16}	0.0189	-0.0053	$\cdots$	-0.0358	$\cdots$
ν_{28}	$\cdots$	$\cdots$	-0.0047	$\cdots$	$\cdots$

TABLE XVI. On-diagonal linear-quadratic coupling constants $\iota_{ij}^{(m)}$ (in eV) for the normal modes of cyclopentanone.

$\iota_{ij}^{(1)}$	ν_1^2	ν_3^2	ν_8^2	ν_{16}^2	ν_{28}^2
ν_1	$\cdots$	$\cdots$	$\cdots$	$\cdots$	$\cdots$
ν_3	$\cdots$	$\cdots$	$\cdots$	$\cdots$	$\cdots$
ν_8	0.0056	0.0021	-0.0096	-0.0073	-0.0012
ν_{16}	$\cdots$	$\cdots$	$\cdots$	$\cdots$	$\cdots$
ν_{28}	-0.0230	-0.0048	-0.0020	-0.0079	$\cdots$
$\iota_{ij}^{(2)}$	ν_1^2	ν_3^2	ν_8^2	ν_{16}^2	ν_{28}^2
ν_1	$\cdots$	$\cdots$	$\cdots$	$\cdots$	$\cdots$
ν_3	$\cdots$	$\cdots$	$\cdots$	$\cdots$	$\cdots$
ν_8	0.0077	0.0045	-0.0082	-0.0018	$\cdots$
ν_{16}	$\cdots$	$\cdots$	$\cdots$	$\cdots$	$\cdots$
ν_{28}	-0.0169	-0.0044	$\cdots$	-0.0109	$\cdots$
$\iota_{ij}^{(3)}$	ν_1^2	ν_3^2	ν_8^2	ν_{16}^2	ν_{28}^2
ν_1	$\cdots$	$\cdots$	$\cdots$	$\cdots$	$\cdots$
ν_3	$\cdots$	$\cdots$	$\cdots$	$\cdots$	$\cdots$
ν_8	0.0100	0.0028	-0.0089	-0.0077	$\cdots$
ν_{16}	$\cdots$	$\cdots$	$\cdots$	$\cdots$	$\cdots$
ν_{28}	-0.0122	-0.0010	$\cdots$	$\cdots$	$\cdots$
$\iota_{ij}^{(4)}$	ν_1^2	ν_3^2	ν_8^2	ν_{16}^2	ν_{28}^2
ν_1	$\cdots$	$\cdots$	$\cdots$	$\cdots$	$\cdots$
ν_3	$\cdots$	$\cdots$	$\cdots$	$\cdots$	$\cdots$
ν_8	0.0049	0.0042	-0.0101	-0.0074	$\cdots$
ν_{16}	$\cdots$	$\cdots$	$\cdots$	$\cdots$	$\cdots$
ν_{28}	-0.0087	0.0022	$\cdots$	-0.0086	$\cdots$

TABLE XVII. On-diagonal quartic coupling constants $\epsilon_i^{(m)}$ (in eV) for the normal modes of cyclopentanone.

i	$\epsilon_i^{(1)}$	$\epsilon_i^{(2)}$	$\epsilon_i^{(3)}$	$\epsilon_i^{(4)}$
ν_1	0.0237	0.0370	0.0159	0.0223
ν_3	0.0049	0.0100	0.0018	0.0019
ν_8	0.0006	0.0005	0.0002	0.0013
ν_{16}	-0.0001	-0.0029	0.0052	0.0003
ν_{28}	$\cdots$	$\cdots$	$\cdots$	$\cdots$

2. Electronic Off-diagonal Parameters

TABLE XVIII. Off-diagonal linear coupling constants $\lambda_i^{(m,l)}$ (in eV) for the normal modes of cyclopentanone.

i	$\lambda_i^{(2,3)}$	$\lambda_i^{(2,4)}$	$\lambda_i^{(3,4)}$
ν_1	0.1572	$\cdots$	0.0821
ν_3	-0.0838	$\cdots$	-0.0156
ν_8	$\cdots$	-0.1206	$\cdots$
ν_{16}	-0.2237	$\cdots$	-0.0497
ν_{28}	$\cdots$	0.0620	$\cdots$

TABLE XIX. Off-diagonal bilinear coupling constants $\mu_{ij}^{(m,l)}$ (in eV) for the normal modes of cyclopentanone.

$\mu_{ij}^{(2,3)}$	ν_1	ν_3	ν_8	ν_{16}	ν_{28}
ν_1	$\cdots$	$\cdots$	-0.0024	$\cdots$	-0.0203
ν_3	$\cdots$	$\cdots$	-0.0011	$\cdots$	-0.0057
ν_8	-0.0024	-0.0011	$\cdots$	$\cdots$	$\cdots$
ν_{16}	$\cdots$	$\cdots$	$\cdots$	$\cdots$	0.0063
ν_{28}	-0.0203	-0.0057	$\cdots$	0.0063	$\cdots$
$\mu_{ij}^{(2,4)}$	ν_1	ν_3	ν_8	ν_{16}	ν_{28}
ν_1	-0.0052	$\cdots$	$\cdots$	0.0150	$\cdots$
ν_3	$\cdots$	0.0042	$\cdots$	-0.0082	$\cdots$
ν_8	$\cdots$	$\cdots$	0.0037	$\cdots$	-0.0221
ν_{16}	0.0150	-0.0082	$\cdots$	-0.0081	$\cdots$
ν_{28}	$\cdots$	$\cdots$	-0.0221	$\cdots$	$\cdots$
$\mu_{ij}^{(3,4)}$	ν_1	ν_3	ν_8	ν_{16}	ν_{28}
ν_1	$\cdots$	$\cdots$	0.0085	$\cdots$	$\cdots$
ν_3	$\cdots$	$\cdots$	-0.0022	$\cdots$	0.0105
ν_8	0.0085	-0.0022	$\cdots$	$\cdots$	$\cdots$
ν_{16}	$\cdots$	$\cdots$	$\cdots$	$\cdots$	$\cdots$
ν_{28}	$\cdots$	0.0105	$\cdots$	$\cdots$	$\cdots$

TABLE XX. Off-diagonal linear-quadratic coupling constants $\eta_{ij}^{(m,l)}$ (in eV) for the normal modes of cyclopentanone.

$\eta_{ij}^{(2,3)}$	ν_1^2	ν_3^2	ν_8^2	ν_{16}^2	ν_{28}^2
ν_1	$\cdots$	-0.0007	-0.0028	-0.0007	-0.0037
ν_3	$\cdots$	-0.0049	0.0006	0.0029	0.0049
ν_8	$\cdots$	$\cdots$	$\cdots$	$\cdots$	$\cdots$
ν_{16}		-0.0012	0.0005	0.0118	0.0004
ν_{28}	$\cdots$	$\cdots$	$\cdots$	$\cdots$	$\cdots$
$\eta_{ij}^{(2,4)}$	ν_1^2	ν_3^2	ν_8^2	ν_{16}^2	ν_{28}^2
ν_1	$\cdots$	$\cdots$	$\cdots$	$\cdots$	$\cdots$
ν_3	$\cdots$	$\cdots$	$\cdots$	$\cdots$	$\cdots$
ν_8	0.0049	0.0021	0.0071	0.0002	$\cdots$
ν_{16}	$\cdots$	$\cdots$	$\cdots$	$\cdots$	$\cdots$
ν_{28}	-0.0087	-0.0010	$\cdots$	$\cdots$	$\cdots$
$\eta_{ij}^{(3,4)}$	ν_1^2	ν_3^2	ν_8^2	ν_{16}^2	ν_{28}^2
ν_1	-0.0062	$\cdots$	-0.0003	0.0006	-0.0012
ν_3	-0.0086	0.0041	0.0007	0.0017	-0.0009
ν_8	$\cdots$	$\cdots$	$\cdots$	$\cdots$	$\cdots$
ν_{16}	0.0007	-0.0045	-0.0003	0.0005	$\cdots$
ν_{28}	$\cdots$	$\cdots$	$\cdots$	$\cdots$	$\cdots$

III. BASIS SET

Diffuse functions optimally contracted for each molecule from a primitive set of 8s8p8d were constructed according to the prescription of Roos.[1] The exponents given in Tab. XXI are from the universal Gaussian basis sets for representation of Rydberg and continuum states by Kaufmann.[2] Tabs. XXII and XXIII collect the contraction coefficients for three sets of diffuse functions for cyclobutanone and cyclopentanone respectively. The diffuse functions were placed on a ghost atom in the charge centroid of the ground cationic state determined from LoProp charges[3] calculated in MOLCAS 6.4.[4]

TABLE XXI. Exponents for the primitive basis functions for three values of angular momentum l and eight values of the principal quantum number n.

n	$l = 0\ (s)$	$l = 1\ (p)$	$l = 2\ (d)$
2.0	0.02462393	0.04233528	0.06054020
2.5	0.01125334	0.01925421	0.02744569
3.0	0.00585838	0.00998821	0.01420440
3.5	0.00334597	0.00568936	0.00807659
4.0	0.00204842	0.00347568	0.00492719
4.5	0.00132364	0.00224206	0.00317481
5.0	0.00089310	0.00151064	0.00213712
5.5	0.00062431	0.00105475	0.00149102

TABLE XXII. Contraction coefficients for three sets of diffuse functions for cyclobutanone.

$l = 0$ (s)		
0.18757690	-0.66901176	0.84247489
1.02138077	-0.78473105	0.22173456
-0.43425367	1.16965432	-2.06764134
0.36093788	0.54692212	-0.48159425
-0.02660994	-0.06342005	1.66260101
-0.28561643	0.02697933	0.84767931
0.29491969	0.02931525	-0.64237097
-0.10167962	-0.01953191	0.24267274
$l = 1$ (p)		
0.28733454	-0.51482697	0.51694331
0.59336328	-0.44690850	0.16166798
0.01309852	0.66233366	-1.02008576
0.43319267	-0.28557390	0.52617583
-0.52217482	1.71767160	-2.19954435
0.49010121	-1.54212007	3.90540389
-0.28532868	0.97402587	-1.77209367
0.07604473	-0.26767560	0.57951653
$l = 2$ (d)		
0.13417940	-0.21298673	0.23409036
0.26292179	-0.24606889	0.19986112
0.36090055	-0.23334084	0.05457146
0.32203482	-0.06405318	0.00085129
0.07999795	0.47688100	-0.96575675
-0.00353851	0.50476530	0.07905963
0.02622863	0.02637718	0.11480124
-0.01171333	0.07072576	1.02575722

TABLE XXIII. Contraction coefficients for three sets of diffuse functions for cyclopentanone.

$l = 0 \ (s)$		
0.00418467	-0.38848697	0.55908927
1.18993678	-1.26254802	0.90072528
-0.46431864	1.24271128	-2.21416585
0.41221310	0.59751973	-0.98671842
-0.02661507	-0.01247047	1.70203509
-0.33434677	0.09202366	1.06594946
0.34380467	-0.04535688	-0.64214518
-0.11840101	0.00656561	0.24234048
$l = 1 \ (p)$		
0.27725230	-0.61352243	0.65451483
0.53090715	-0.27833537	-0.10891805
0.12051661	0.42258781	-0.73894617
0.35196052	0.00376434	0.12462769
-0.41598528	1.34057797	-1.44956674
0.39835946	-1.18216962	3.11862406
-0.23366103	0.75511770	-1.31887282
0.06236085	-0.20643878	0.43609035
$l = 2 \ (d)$		
0.16439619	-0.32105070	0.35040189
0.27597911	-0.27560551	0.19803434
0.33584271	-0.14156831	-0.09950192
0.31715460	0.01710969	-0.16583083
0.08042406	0.47698256	-0.78001504
-0.00479743	0.43481886	0.20066895
0.02559397	-0.01114904	0.44671880
-0.01121493	0.06198461	0.62692971

REFERENCES

[1] B. O. Roos et al., Multiconfigurational Perturbation Theory: Applications in Electronic Spectroscopy, in *New Methods in Computational Quantum Mechanics*, volume 93 of *Adv. Chem. Phys.*, pages 219–331, John Wiley & Sons Inc., New York, 1996.

[2] K. Kaufmann, W. Baumeister, and M. Jungen, J. Phys. B: At. Mol. Opt. Phys. **22**, 2223 (1989).

[3] L. Gagliardi, R. Lindh, and G. Karlström, J. Chem. Phys. **121**, 4494 (2004).

[4] G. Karlström et al., Comp. Mater. Sci. **28**, 222 (2003).